A Molecular Dynamics Investigation of Hydrolytic Polymerization in a Metal−Hydroxide Gel

James R. Rustad*,† and William H. Casey†,‡

Department of Geology and Department of Chemistry, University of California, Davis, One Shields Avenue, Davis, California 95616

Received: August 5, 2005; In Final Form: February 2, 2006

The early stages of the spontaneous hydrolytic polymerization of an active hydroxide in the anti-bayerite structure are followed by using molecular dynamics simulations. The polymer populations are calculated as a function of reaction progress and compared with a model governed by purely random bonding. In agreement with experimental observations in aqueous solutions, the transformation of singly bridged to doubly bridged metal ions is shown to have a significant autocatalytic component. The overall polymer populations, however, are very close to the predictions of the random bonding model, indicating that local autocatalytic behavior is decoupled from multimer populations at the larger scales. The calculations show that solid-state transformation processes do not preferentially give rise to higher order multimers, and suggest that interfacial processes, involving bulk solution, are required to facilitate rapid transformation to higher order oligomers. Two reaction pathways are identified for the dewatering of μ-H_3O_2 bridges into μ-OH bridges. Both are activated primarily by undercoordination of one of the metals centers involved in the bridge.

1. Introduction

The hydrolysis of dissolved trivalent metals to form minerals and amorphous solids is among the most important processes in environmental chemistry. These gels and colloids move with subsurface water and accumulate in soils. Little is understood about this process beyond the very earliest stages.[1,2] The barriers to progress are 2-fold: First, hydrolysis generally proceeds so rapidly that it is impossible to isolate the reaction products and study their formation rates; the reaction branches quickly. Second, the rates and products of hydrolysis are sensitive to the initial conditions; if experiments are conducted in solutions that are sufficiently dilute to control the reaction, the products differ from those in less-dilute solutions.

A way to alleviate the sensitivity to initial conditions was indicated by Spiccia and Marty,[3] who examined the aging of an "*active-hydroxide*" solid, which consists of a hydrogen-bonded structure of linked $Cr(OH)_3(OH_2)_3$ moieties. The active-hydroxide solid has an anti-bayerite structure (Figure 1a) and forms when the pH is raised rapidly in a solution containing hexahydrated metals that are inert to ligand exchange (e.g., $Cr(H_2O)_6^{3+}$, $Rh(H_2O)_6^{3+}$). Raising pH causes three of the bound waters to deprotonate rapidly and form bound hydroxyls. The resulting neutral complexes crystallize into an ordered lattice with their inner-coordination spheres intact. Each complex donates, and accepts, three hydrogen bonds to, and from, neighbors, so that the structure is held together by $OH{\cdot}OH_2^-$ (hereafter written $H_3O_2^-$) bridges between M(III) sites.

With time, small oligomers form as the $M(OH)_3(H_2O)_3$ units in the structure react to convert the μ-H_3O_2 bridges to μ-OH bridges via a reaction that releases water:

$$>M-(\mu\text{-}H_3O_2)-M< = >M-(\mu\text{-}OH)-M< + H_2O$$

This process displaces the reacting metals from their stable lattice positions (Figure 1b). The polymerization reaction can be quenched by acidification, releasing the oligomers intact to the solution. This method was used to follow the polymerization of Cr(III)-active hydroxide.[3] The products included dimers, trimers, and tetramers that can be distinguished by using ion-exchange chromatography and optical spectroscopy, as well as larger oligomers (pentamers and above) that could not be cleanly separated from one another and were lumped into a single class. Reference 3 reports that an unexpectedly high concentration of large oligomers forms quickly in the aging of the active hydroxide, which inspired our search for autocatalysis.

The formation of oligomers within the active-hydroxide structure could be favored for two reasons. First, all metals in the active-hydroxide structure are $H_3O_2^-$ bridged, so monomers are prearranged to react and form μ-OH; the $H_3O_2^-$ bridge might be regarded as a key precursor to forming bridged complexes.[4−6] Second, the $M(OH)_3(H_2O)_3$ constituents are all uncharged and both rates and equilibrium constants for oligomerization increase as electrostatic repulsion is reduced (Table 1) as the number of inner-sphere hydroxyls is increased.[7]

Using molecular-dynamics (MD) simulations, we test here the hypothesis that the reaction is autocatalytic, that is, displacement of an M(III) atom by a bridge and release of a bound water accelerates subsequent bonding and favors large oligomers. Experimental data show rapid formation of higher order oligomers suggesting autocatalysis, as we discuss below. To test the hypothesis we compare two simulation cases: (i) a model in which oligomers form randomly on a fixed lattice isostructural with the active hydroxide and (ii) a fully reactive molecular dynamics simulation where bound ligands and free waters can dissociate in response to local chemical conditions. We expect that autocatalysis will produce a collection of higher order oligomers that is much different than would be predicted by random bonding, as was implied in the experiments.

† Department of Geology.
‡ Department of Chemistry.

10.1021/jp054379t CCC: $33.50 © 2006 American Chemical Society
Published on Web 03/18/2006

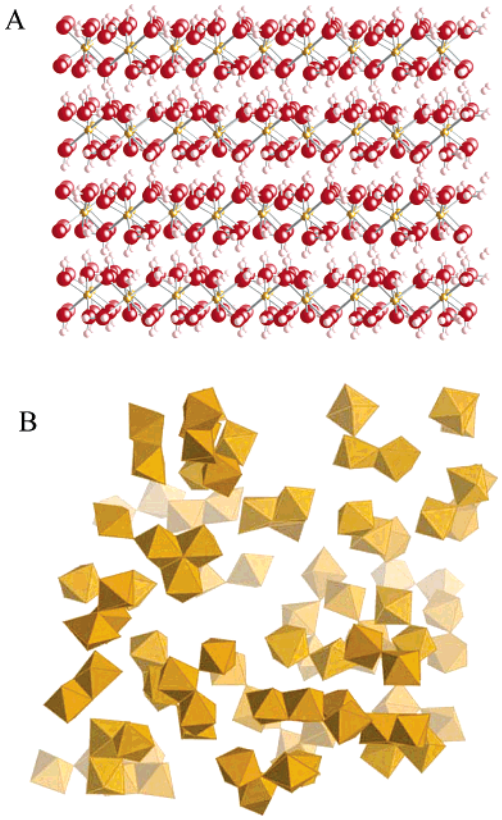

Figure 1. (Top) The starting condition was a lattice of 216 $M(OH)_3(H_2O)_3$ units, each hydrogen bonded to a neighbor in the anti-bayerite lattice (see ref 27). Each unit both donates to and accepts from the neighbors three hydrogen bonds. (Bottom) After considerable reaction, the structure has polymerized to form various oligomers, here shown in polyhedral representation, with μ_2-OH and μ_3-OH bridges. Both the monomeric species and the released water molecules are eliminated for clarity.

TABLE 1: Rate Coefficients for Formation of $(H_2O)_4Cr(\mu\text{-}OH)(H_2O)_4OH^{4+}$ from Various Reactants at 298 K and (from ref 6)

reactants	k (M^{-1} s^{-1})
$Cr(H_2O)_6^{3+} + Cr(H_2O)_6^{3+}$	not determined
$Cr(H_2O)_6^{3+} + Cr(H_2O)_5OH^{2+}$	6×10^{-6}
$Cr(H_2O)_5OH^{2+} + Cr(H_2O)_5OH^{2+}$	2×10^{-4}
$Cr(H_2O)_4(OH)_2^{+} + Cr(H_2O)_5OH^{2+}$	3.8×10^{-2}
$Cr(H_2O)_4(OH)_2^{+} + Cr(H_2O)_4(OH)_2^{+}$	1.8

2. Methods

2.1. Potential Functions. The simulations were carried out with previously developed Fe−O−H interaction potentials.[8] The O−O, O−H, and H−H interactions are taken from ref 9 without modification. The functional form of this potential is basically that of Stillinger and David.[10,11] The model consists of +1 and −2 charges on the proton and the oxide ion, and an inducible point dipole centered on the oxygen ion. The potential differs from other water potentials in that the point dipole responds to the electric field from all protons including intramolecular protons. As described in more detail in ref 9, short-ranged O−H interactions are applied to recover the known structure, heterolytic dissociation energy, dipole moment, and vibrational frequencies of the isolated water molecule. The O−O interactions were chosen to reproduce as closely as possible the O−O radial distribution function.[12]

The model is capable of reproducing quite realistic acid/base speciation: a free proton in water yields a combination of Eigen $(H_3O)\cdot 3H_2O^+$ and Zundel $H_5O_2^+$ structures, with the Eigen structure predominating, in agreement with ab initio[13] and EVB[14] molecular dynamics calculations. The free hydroxide ion yields an $OH(H_2O)_4^-$ species in solution, in agreement with experiment,[15] and first-principles methods.[16] The model also performs reasonably well for relevant gas-phase clusters: relevant to this study is the hydroxide affinity of water. The energy for the reaction $H_3O_2^- \rightarrow H_2O + OH^-$ is 38.1 kcal/mol. This compares with 37.6 kcal/mol at the DFT BP/DZVP2 level.[17]

As described in more detail in ref 8, the M−O potential function was fitted to quantum mechanical calculations on the Fe^{3+}−(single) H_2O potential surface.[18] The functional form allows for polarization of bound water molecules by the M^{3+} ion. This polarization lowers the *induced* dipole moment of bound water molecules, increasing the total dipole moment (the induced moment in the oxide ion is pointed in the opposite direction to the overall moment, away from the intramolecular protons). Subsequent research has shown that the potential should be taken as being broadly appropriate for trivalent metals with M−O bond lengths of 1.9−2.1 Å, rather than being assigned to a particular metal, like Fe^{3+}. One reason for this retreat is that hydrolysis constants for trivalent ions do not correlate with bond lengths.[19] The fact that the trivalent metals do not show a size-charge correlation must reflect more complex bonding that cannot be captured in a straightforward way by using ionic models such as the ones used here. Thus, in this paper we refer to a generic M(III) complex and not Fe(III).

Again, both gas-phase and solution-phase speciation are reasonably accurate for trivalent metals as a whole, and the model has been used to study a wide range of problems from the hydroxylation of α-Fe_2O_3,[20] to the effect of hydrolysis on electron-transfer rates between ferrous and ferric ion in aqueous solution,[21] to the exchange of hydroxide ions on large aluminum polyoxocations.[22] The Stillinger−David approach has recently been used to look at proton transport in ion channels.[23] Models such as these are quite capable of describing chemical reactions with approximately correct energetics, as long as the products are heterolytic.

2.2. Protocol. Molecular-dynamic (MD) simulations were carried out from an initial condition of 216 $M(OH)_3(H_2O)_3$ units arranged in a periodic anti-bayerite structure (Figure 1, top) in a 30.09 Å × 30.38 Å × 32.64 Å box. The simulation was run for $\sim 3.5 \times 10^{-9}$ s (1.3×10^6 time steps at 0.27×10^{-15} s per time step) at 300 K. The NVT ensemble was implemented by using Nose−Hoover methods, and polarization was treated with use of extended Lagrangian methods.[24] Program units are in MDU (mass = proton mass, length = Å, charge = e). The mass of the ion thermostat was set at 50 MDU, the mass of the dipole thermostat (T = 5 K) was set at 10 MDU, and the fictitious dipole mass was set at 0.1 MDU. In the Parrinello−Rahman calculations[25] described below, the mass of the lattice degrees of freedom was set at 200 MDU. During the simulation, the $M(OH)_3(H_2O)_3$ units reacted with one another and polymerized to form a set of oligomers that were counted separately and organized according to structure and molecular lifetime.

As a baseline for comparison we also follow the formation of oligomers from the active-hydroxide structure by randomly adding bonds, limited to no more than six to a given M(III) site, to one of the eight nearest M(III) neighbors in the structure. For this purpose, we used a lattice of 89 664 iron atoms (dimension 255.76 Å × 212.63 Å × 228.51 Å). The resulting oligomers were organized according to structure and size to compare with the MD simulations.

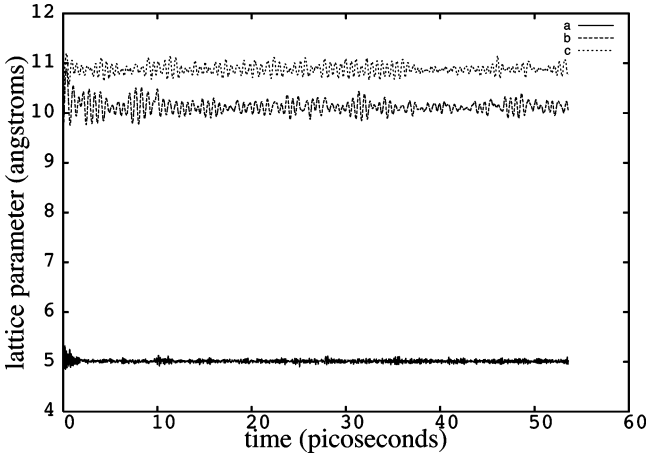

Figure 2. Baseline lattice parameters (a, b, c) (Å) for $M(OH)_3(H_2O)_3$ in the anti-bayerite structure as a function of time (picoseconds) obtained from the Parrinello−Rahman method as a function of time. The conditions correspond to zero pressure and 100 K. The angles between the lattice vectors (not shown) maintain themselves at an average of 90°.

3. Results

3.1. Active-Hydroxide Structure. To create the initial conditions for the polymerization, and to establish a benchmark for the potentials, we checked the stability of $M(OH)_3(H_2O)_3$ [or, equivalently, $M(H_3O_2)_3$] in the anti-bayerite structure using the model potentials and constant-stress molecular dynamics calculations. To generate the active-hydroxide structure, we began with the structure of bayerite.[26] A conformer search was then carried out as follows: Aluminum ions were placed on the appropriate sublattice to create the anti-bayerite structure, while another sublattice of aluminum ions was replaced with three protons, randomly distributed on a sphere, radius 1 Å, centered on the removed aluminum ion. The fractional coordinates of the protons were then optimized, holding both the metal and oxygen coordinates fixed. A list was kept of the top five structures whose coordinates were reused by making random displacements of the protons from the start (at an average distance of 0.2 Å). The best structure after 100 000 iterations was retained and then subjected to 10 heating and cooling cycles (10 ps per cycle between 750 and 300 K). From this structure, Parrinello−Rahman[25] molecular-dynamics simulations were carried out at 100 K to check the stability of the lattice. The values of **a**, **b**, and **c** at zero pressure and 100 K are shown in Figure 2. Not shown are the values of α, β, and γ, which fluctuate within a couple of degrees of 90°. The structure is stable, but differs somewhat from the $Cr(H_3O_2)_3$ structure described in ref 27. In our calculations the hexagonal sheet distorts into an orthorhombic mesh with one of the hexagonal distances relaxing to 5.65 Å and the other relaxing to 5.02 Å. In $Cr(H_3O_2)_3$ these distances are both 5.31 Å. In our model, the repeat distance in the *c* crystallographic direction is doubled and distorted into two distances 5.37 and 5.54 Å. These differences could be a result of our structure being proton ordered and the experimental structure being disordered. More crystallographic work would be required before further comparisons are warranted.

In our proton-ordered structure, the hydrogen-bonding patterns are complex and variable in terms of the O−O and OH−O distances (Figure 3). The structure consists of sheets in the **a**−**b** plane connected by tight HO−H−OH hydrogen bonds in the **a** direction (O−O distance 2.51 Å and HO−H distances of 1.28 and 1.23 Å) (see Figure 3A). We regard the connectivity in the

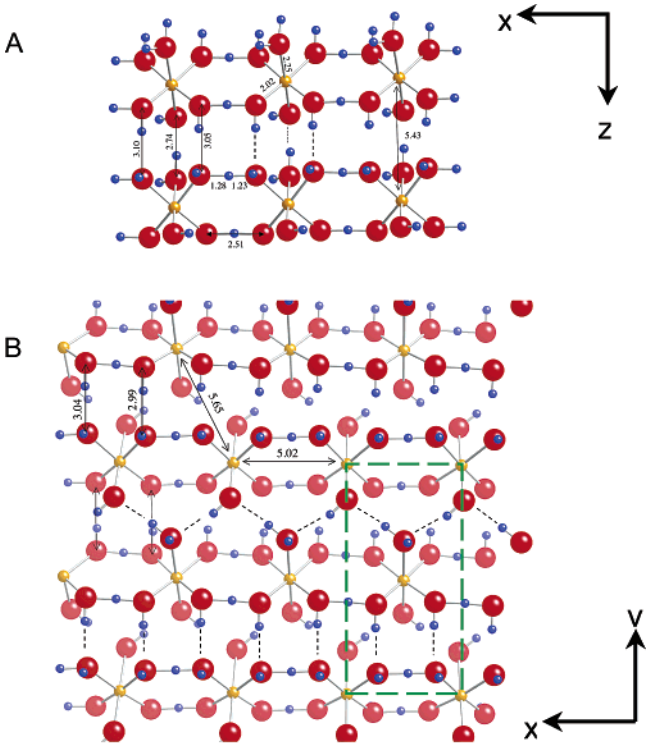

Figure 3. Details of the hydrogen-bonding networks in the ordered active-hydroxide structure. Hydrogen bonds are noted as dashed lines. (a) View showing the layered structure with sets of hydrogen bonds and key distances. (b) View perpendicular to the layer with the unit cell outlined in green.

a direction in terms of rows of edge-sharing $M(H_3O_2)_6$ octahedra. Successive rows are offset by $^1/_2$**a** and bound to each other by corrugated chains of HO···HOH (i.e., with the central proton located asymmetrically between the hydrogen-bound oxygens) parallel to **a**, as well as cross-links, also asymmetric, in the **b** direction. Connections from one sheet to the other are made by doubly bridging, asymmetric hydrogen bonds (Figure 3B) in face-sharing arrangements (i.e., each metal ion shares three μ-H_3O_2 bridges).

3.2. Polymerization of the Active-Hydroxide Structure. As the 100 K structure is heated above 300 K (now keeping the lattice vectors fixed at their 100 K values), polymerization is induced by reactions that eliminate water molecules from the $H_3O_2^-$ bridges to create μ_2-OH hydroxyl bridges. The release of water molecules becomes a useful progress variable since, at completion of polymerization, the released waters are three times the number of total metals in the simulation. Here we define the reaction progress in the MD simulations as ζ = no. of free waters/(3 × no. of metal ions), which would vary from $\zeta = 0$ to 1 as the polymerization begins and reaches completion. The progressive changes in bonding from oligomer formation are summarized in the radial-distribution function for M−M distances shown in Figure 4. The ⟨M−M⟩ distance of ∼5.6−5.8 Å corresponds to the $H_3O_2^-$ bridged structure of the starting active-hydroxide structure. As one can see, this peak decreases with time as inner-sphere μ_2-OH bridges form, resulting in two peaks. One peak near the ⟨M−M⟩ distance of ∼3.9 Å corresponds to two metals linked by a single μ_2-OH bridge and these grow with time as the structure polymerizes. A second peak near ⟨M−M⟩ ∼ 3.5 Å corresponds to metals that are linked to a neighbor by two μ_2-OH bridges.

The integrated areas of these two peaks are proportional to the number of μ_2-OH bridges and they are subequal in concentration to one another (Figure 4). This point is important

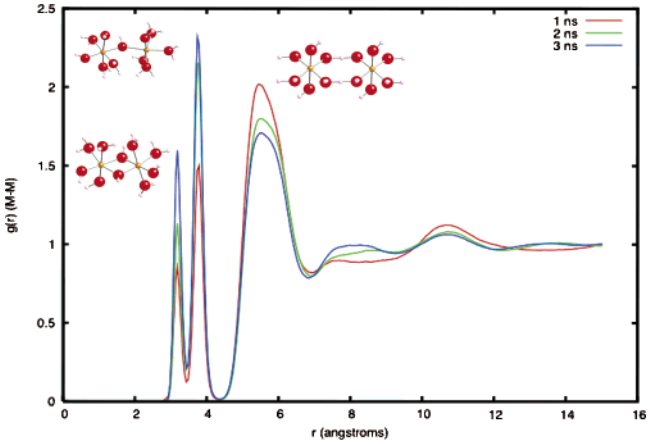

Figure 4. The radial-distribution function [g(r)] for M−M distances as a function of time in the simulations. The distributions shown represent averages over 10^6 time steps in windows centered on 1, 2, and 3 ns. The ⟨M−M⟩ distance of $r \sim 5.6-5.8$ Å corresponds to the $H_3O_2^-$ bridged structure of the starting active-hydroxide structure. The peak near the ⟨M−M⟩ distance of $r \sim 3.9$ Å corresponds to two metals linked by a single μ_2-OH bridge and a second prominent peak near $r \sim 3.5$ Å corresponds to metals that are linked to a neighbor by two μ_2-OH bridges.

because, as we discuss below, approximately equal concentrations of single- and double-bridged dimers do not arise from the random model for polymerization. The MD simulation indicates that M(III) oligomers preferentially link to one another via two μ_2-OH bridges after a single bridge initially forms. This favoring of double bridges is a notable departure from random bonding. In the random bonding model, for example, the dimer population peaks near $\zeta = 0.1$, whereas in the molecular dynamics simulations the dimer population reaches its peak somewhat later at $\sim\zeta = 0.16$.

However, overall the MD simulations produced an oligomer ensemble that closely resembles the random-bonding case (Figure 2b). There is no evidence for autocatalysis at this scale. The progression of oligomers is uniform in the early stages and closely resembles a random process where there is no inherent preference for higher order oligomers. As the reaction progresses, of course, small oligomers disappear as higher order oligomers form until the structure is virtually polymerized into an metal−hydroxide gel. At a finer scale the MD simulations yield a different ensemble of molecular structures than the random model. The rapid formation of double bridges is most evident, both in the g(r) function shown in Figure 4 and also in the ensemble of dimers shown in Figure 6, but the structures of the larger oligomers formed in the MD simulation also appear to differ markedly from the random model (data not shown). In particular, the number of metals linked by double μ_2-OH bridges is higher in the MD simulation and including ring trimers (data not shown). Because the number of higher order oligomers is so small even in these large MD simulations, it is difficult to demonstrate an unequivocal difference to the random model. Qualitatively, however, the structures appear different; for example, the random model favors linear molecules with fewer double μ_2-OH bridges and ring compounds.

3.3. Reaction Trajectories. The condensation reaction to form M−(OH)−M was always initiated by loss of a water molecule from one of the M^{3+} sites. As shown in Figures 7 and 8, two paths were observed. The most common path, shown in Figure 7, involved loss of an equatorial or axial water and then the formation of a face-sharing structure (Figure 7c) typically with two H_3O_2 bridges and one OH−OH contact. The undercoordinated metal center becomes a trigonal bipyramid

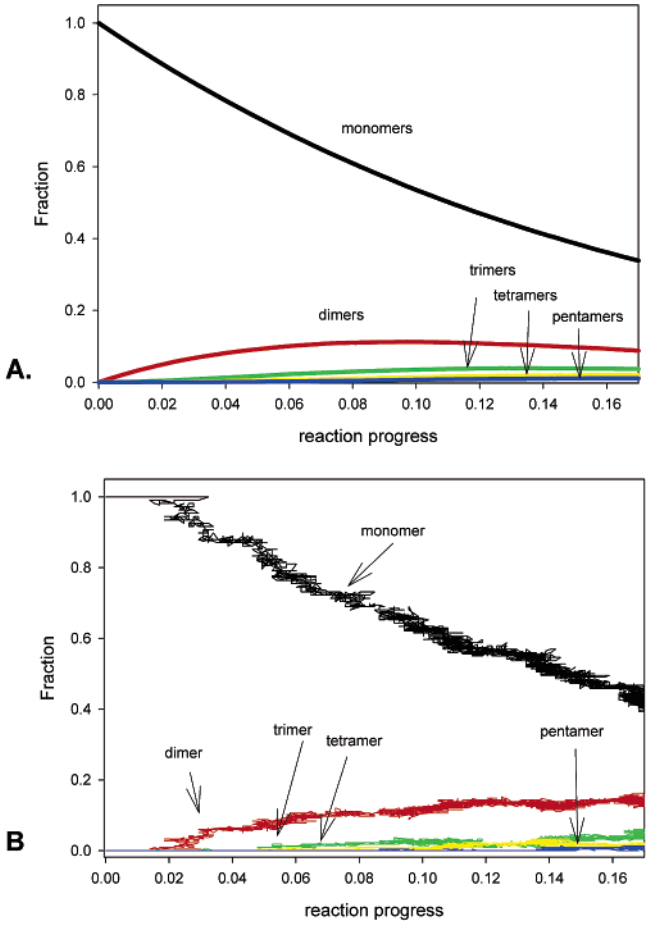

Figure 5. (a) The collection of oligomers as a function of time for random bonding between $M(OH)_3(H_2O)_3$ units in the active-hydroxide structure. (b) The collection of oligomers using the MD method with a more realistic potential for bonding that includes protonation, deprotonation, and hydrolysis. The reaction progress variable is defined in section III B.

having one shared face with the octahedral ion. This structure was metastable on time scales of approximately 0.5 ps. This period of metastability typically involves several protonation−deprotonation events in which the identity of the H_3O_2 and OH−OH bridges changes, until the hydroxyl of the trigonal-bipyramid metal center rotated into octahedral position, and the hydroxl attaches to the undercoordinated metal center.

A second mechanism was observed involving direct breaking of the H_3O_2 linkage. In this mechanism, shown in Figure 8, one of the metal centers in a di-H_3O_2 bridged complex loses an equatorial water molecule. The H_3O_2 linkage is pulled apart as the undercoordinated center moves toward trigonal-bipyramidal coordination. As the H_3O_2 linkage severs, the water molecule stays on the octahedral ion (it is less acidic because it remains octahedrally coordinated), and this water molecule acts as a nucleophile to the undercoordinated metal center. To complete the reaction, the metastable μ-H_2O bridge must lose a proton to become μ-OH. This last step was sometimes rate-limiting; in several instances, the reaction was observed to completely reverse if no sites were available to receive the proton from the μ-H_2O group. Presumably this step would be easy in an interfacial environment, as the aqueous solution could easily accommodate the proton.

Dimers having one OH bridge and one H_3O_2 bridge are converted to a di-μ-OH structure exclusively through the latter mechanism, shown in Figure 9. This second water-elimination

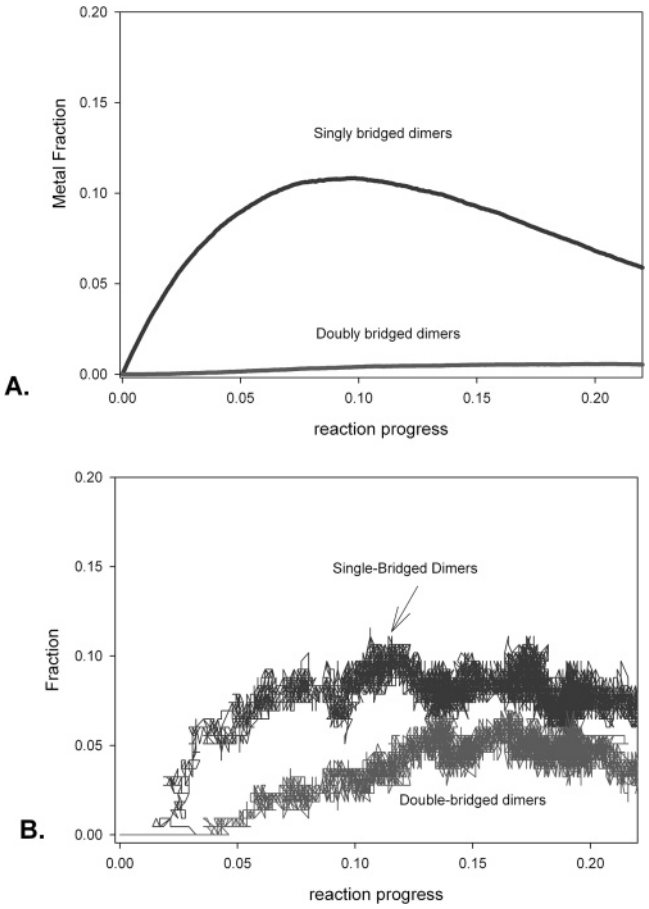

Figure 6. The evolution of singly and double bridged dimers as a function of time produced by random bonding (a) and (b) using the MD method that includes a more comprehensive treatment of bonding. The reaction progress variable is defined in section 3.2.

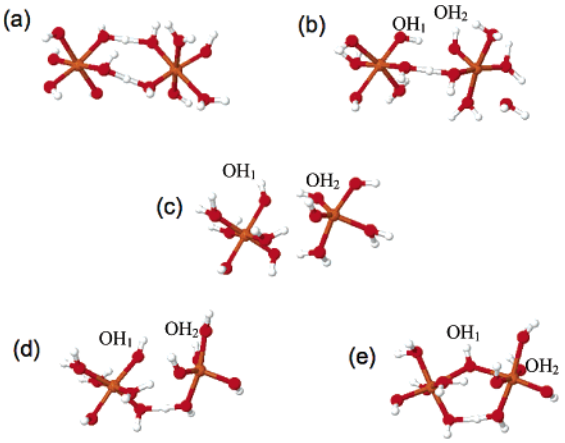

Figure 7. Formation of a single M−OH−M bridge via mechanism 1: (a) formation of a double-H_3O_2 bridged structure, (b) water loss, (c) formation of a face sharing structure with OH_1−OH_2 contact, and (d) rotation of OH_2 and nucleophilic attack of undercoordinate M^{3+} by OH_1.

reaction, however, is accelerated over that shown in Figure 8 because of the additional ring strain from the μ-OH bridge.

4. Discussion

A key feature of the active-hydroxide structure is that the polymerization reaction can be quenched at any time by acidification as protons break the hydrogen bonds. The formed complexes then release intact to the solution. Using this method,

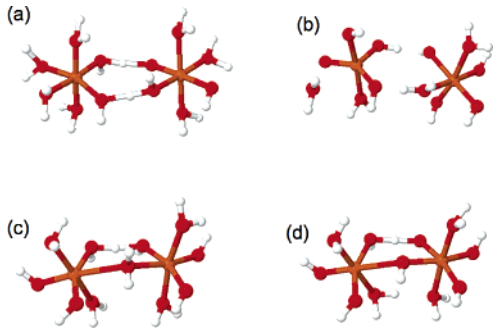

Figure 8. Formation of a single M−OH−M bridge via mechanism 2: (a) double-H_3O_2 bridged structure, (b) water loss, (c) rotation and separation of OH from reacting H_3O_2 complex, and concomitant formation of the μ-(H_2O) group, and (d) proton loss from the μ-(H_2O) group.

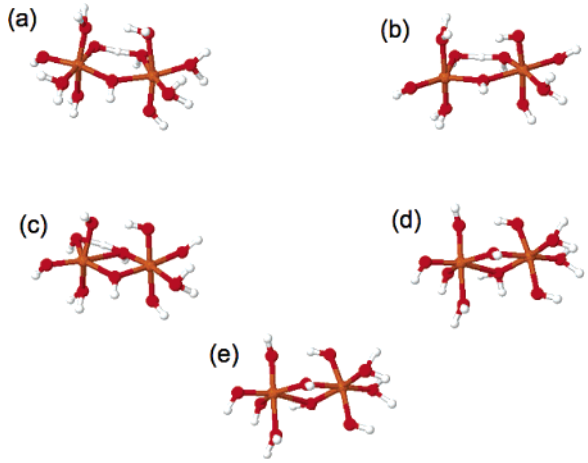

Figure 9. Formation of a second M−OH−M bridge on a singly OH-bridged dimer: (a) formation of a M−(OH)(H_3O_2)−M complex, (b) loss of equatorial water from the left metal center, (c) rotation of the (H_3O_2) bridge toward the position of the lost water molecule and nucleophilic attack of one of the O atoms to the left metal center, (d) formation of the μ-H_2O bridge, and (e) loss of proton from the μ-H_2O bridge.

Spiccia and Marty[3] followed polymerization of Cr(III)-active hydroxide and classified the oligomeric products. Small oligomers, including dimers, trimers, and tetramers, could be distinguished from one another by using ion-exchange chromatography and optical spectroscopy. The concentrations of these molecules were followed as a function of time. Another class included the undifferentiated larger oligomers (pentamers and above) that could not be cleanly separated from one another. These authors had two important conclusions. First, they found that an unexpectedly high concentration of large oligomers forms quickly in the aging of the active hydroxide, which inspired our search for autocatalysis via simulation. Second, they concluded that bulk solution in contact with the active-hydroxide solid might be essential. They reached this conclusion from the qualitative similarity between the pH dependence of the solid solubility and the pH dependence of oligomer formation. The solid was soluble at extreme pH conditions where oligomer formation was most rapid.

In our simulations, we have no bulk solvent and do not vary pH. However, the striking result of the simulations is that the collection of oligomers formed by solid-state aging is nearly indistinguishable from that formed by random assignment of bonds. These observations support the conclusion of ref 3 that the higher order oligomers are favored only where there is bulk solvent to facilitate polymerization. Once formed in solution,

the large oligomers reattach to the active hydroxide surface and are released by acidification. We see no evidence that the large oligomers form preferentially in the absence of bulk solvent.

The details, however, are considerably different from the predictions of the random-model baseline. Both experimentally and in the MD simulations, dimers with two bridges are considerably favored over those with single bridges (Figure 3). Random assignment of bonds to the active-hydroxide structure strongly disfavors double bridges in the same way that higher order oligomers are disfavored: initially, the concentrations of μ_2-OH scale like the number of bridging bonds in the whole structure: single-bridged dimers are proportional to X, doubly bridged dimers are proportional to X^2, etc., with X being the mole fraction of all potential bonds in the active-hydroxide structure that are filled.

In this sense, the MD simulations reproduce experiment. For example, the equilibrium constant for dissociating a double-bridged dimer to form a single bridge

$$(H_2O)_4Cr(\mu\text{-}OH)_2Cr(H_2O)_4^{4+} + H_2O \rightarrow (H_2O)_5Cr(\mu\text{-}OH)Cr(H_2O_4)(OH)^{4+}$$

is on the order of $K \sim 0.02$ in homogeneous solutions.[6] In the MD simulation the ratio of single-bridged to double-bridged dimers deviates strongly from the random model, but never reaches a ratio as large as that indicated for Cr(III) oligomers at equilibrium, which is perhaps unsurprising. Autocatalysis is indicated only in double-bridge formation, which is true both in simulation and in experiment. If so, then the structure of higher order clusters must differ from that of a random model because the chemistry is expressed in local bonding environments but not in large molecular architectures.

5. Conclusions

To within the accuracy of the molecular-dynamics potential, there is no evidence that higher order oligomers form more quickly than expected from random assignment of bonds in an aging gel with the active-hydroxide structure. However, in both experiment and simulation, we find a high concentration of metal pairs that link to neighbors via two μ-OH bridges. At this scale, bond formation is autocatalytic (one bond favors formation of another) and this local chemistry accounts for the common structures of the small molecules, such as ring trimers, etc. The effects do not extend beyond this local scale. The large oligomer concentrations resemble that predicted by random bond formation because they grow by a combination of repeated monomer addition, which does not affect the overall reactivity of the large cluster, or by linkage of two smaller oligomers to one another by a single linkage. The rate of second bond formation is affected by the first, but the initial linkage does not labilize other bonds in the cluster. Thus, the cluster concentrations resemble the random case.

Acknowledgment. Support to J.R.R. and W.H.C. was from grants from the Basic Energy Sciences division of the U.S. DOE (DE-FG02-05ER15639 (J.R.R.) and DE-FG03-96ER14629 (W.H.C.)) and the US NSF (via EAR 05-15600). Access to computer facilities was provided by the Molecular Sciences Computing Facility of the Environmental Molecular Sciences Laboratory, Pacific Northwest National Laboratory, which is operated for the U.S. Department of Energy by Battelle Memorial Institute under Contract DE-AC06-76RL0 1830.

References and Notes

(1) Schwertman, U.; Friedl, J.; Stanjek, H. *J. Colloid Interface Sci.* **1999**, *209*, 215.
(2) Jolivet, J. P.; Chaneac, C.; Tronc, E. *Chem. Commun.* **2004**, 481.
(3) Spiccia, L.; Marty, L. *Inorg. Chem.* **1986**, *25*, 266.
(4) Ardon, M.; Bino, A. *Inorg. Chem.* **1985**, *24*, 1343.
(5) Bino, A.; Gibson, D. J. *J. Am. Chem. Soc.* **1982**, *104*, 4383.
(6) Springborg, J. *Adv. Inorg. Chem.* **1988**, *32*, 55.
(7) Crimp, S. J.; Spiccia, L.; Krouse, H. R.; Swaddle, T. W. *Inorg. Chem.* **1994**, *33*, 465.
(8) Rustad, J. R.; Hay, B. P.; Halley, J. W. *J. Chem. Phys.* **1995**, *102*, 427.
(9) Halley, J. W.; Rustad, J. R.; Rahman, A. *J. Chem. Phys.* **1993**, *98*, 4110.
(10) Stillinger, F. H.; David, C. W. *J. Chem. Phys.* **1978**, *69*, 1473.
(11) . Stillinger, F. H.; David, C. W. *J. Chem. Phys.* **1980**, *73*, 3384.
(12) Soper, A. K.; Phillips, M. G. *Chem. Phys.* **1986**, *107*, 47.
(13) Marx, D.; Tuckerman, M. E.; Hutter, J.; Parrinello, M. *Nature* **1999**, *397*, 601.
(14) Schmitt, V. W.; Voth, G. A. *J. Chem. Phys.* **1999**, *111*, 9361.
(15) Botti, A.; Bruni, F.; Imberti, S.; Ricci, M. A.; Soper, M. A. *J. Mol. Liq.* **2005**, *117*, 81.
(16) Tuckerman, M. E.; Marx, D.; Parrinello, M. *Nature* **2002**, *417*, 925.
(17) Dixon, D. A. Unpublished.
(18) Curtiss, L. A.; Halley, J. W.; Hautman, J.; Rahman, A. *J. Chem. Phys.* **1987**, *86*, 2319.
(19) Brown, P. L.; Sylva, R. N.; Ellis, J. *J. Chem. Soc., Dalton Trans.* **1985**, 723.
(20) Henderson, M. A.; Joyce, S. A.; Rustad, J. R. *Surf. Sci.* **1998**, *417*, 66.
(21) Rustad, J. R.; Rosso, K. M.; Felmy, A. R. *J. Chem. Phys.* **2004**, *120*, 7607.
(22) Rustad, J. R.; Loring, J. S.; Casey, W. H. *Geochim. Cosmochim. Acta* **2004**, *68*, 3011.
(23) Chakrabarti, N.; Roux, B.; Pomes, R. *J. Mol. Biol.* **2004**, *343*, 493.
(24) Saboungi, M. L.; Rahman, A.; Halley, J. W.; Blander, M. *J. Chem. Phys.* **1987**, *88*, 5818.
(25) Parrinello, M.; Rahman, A. *J. Appl. Phys.* **1981**, *52*, 7182.
(26) Zigan, F.; Joswig, W.; Burger, N. *Z. Kristallogr.* **1978**, *148*, 255.
(27) Giovanoli, R.; Stadelmann, W.; Feitknecht, W. *Helv. Chim. Acta* **1973**, *56*, 839.